PCCP

PAPER

Cite this: *Phys. Chem. Chem. Phys.*, 2015, **17**, 24874

Carbon and proton Overhauser DNP from MD simulations and *ab initio* calculations: TEMPOL in acetone†

Sami Emre Küçük,[a] Timur Biktagirov[b] and Deniz Sezer*[a]

Received 27th July 2015,
Accepted 25th August 2015

DOI: 10.1039/c5cp04405g

www.rsc.org/pccp

A computational analysis of the Overhauser effect is reported for the proton, methyl carbon, and carbonyl carbon nuclei of liquid acetone doped with the nitroxide radical TEMPOL. A practical methodology for calculating the dynamic nuclear polarization (DNP) coupling factors by accounting for both dipole–dipole and Fermi-contact interactions is presented. The contribution to the dipolar spectral density function of nuclear spins that are not too far from TEMPOL is computed through classical molecular dynamics (MD) simulations, whereas the contribution of distant spins is included analytically. Fermi contacts are obtained by subjecting a few molecules from every MD snapshot to *ab initio* quantum mechanical calculations. Scalar interaction is found to be an essential part of the ^{13}C Overhauser DNP. While mostly detrimental to the carbonyl carbon of acetone it is predicted to result in large enhancements of the methyl carbon signal at magnetic fields of 9 T and beyond. In contrast, scalar coupling is shown to be negligible for the protons of acetone. The additional influence of proton polarization on the carbon DNP (three-spin effect) is also analyzed computationally. Its effect, however, is concluded to be practically insignificant for liquid acetone.

I. Introduction

Overhauser dynamic nuclear polarization (ODNP) can substantially increase the signal intensity of nuclear magnetic resonance (NMR) measurements in liquids.[1] The effect relies on polarizing the electron spins of dissolved free radicals with the use of microwaves and transferring the large electron polarization to the nuclear spins of the solvent.[2,3] The magnitude of the effect is directly proportional to the gyromagnetic ratio of the electron spin, γ_S, and inversely proportional to the gyromagnetic ratio of the nuclear spin of interest, γ_I. Thus, the smaller the γ_I the larger the relative increase of the NMR signal. In the case of the ^{1}H and ^{13}C nuclear spins examined here, larger ODNP enhancements are expected for the latter because γ_C is four times smaller than γ_H.

Instrumental developments that made possible the use of ODNP in continuous-flow NMR and medical MRI,[4–6] as well as novel applications to biomolecular NMR[7–9] have spurred a revived interest in quantifying the mechanisms responsible for the effect. Recent high-field ODNP experiments, reporting considerable enhancements, were performed for solvents containing ^{1}H,[10–15] ^{13}C,[10,16–18] and ^{19}F.[19,20] These studies demonstrated that while for ^{1}H nuclei the scalar interaction with the electron spin is negligible compared to the dipolar interaction, for the other nuclei both interactions may be of comparable magnitude—a complication known from previous work.[3] Since in the ODNP effect the scalar and dipolar interactions enhance the NMR signal in opposite directions, their simultaneous presence is detrimental to the overall enhancement. Computational approaches capable of quantifying the contributions of these two interaction types and thus predicting the magnitude of the expected enhancement are, therefore, highly desirable.

Previously, we have employed atomistic molecular dynamics (MD) simulations to calculate ^{1}H ODNP coupling factors.[21–24] Being classical in nature, the MD simulations only provide information about the positions of the atomic centers in the simulated liquid solution. Invoking the point-dipole approximation, the atomic positions are used to calculate the dipole–dipole interaction between the electron and nuclear spins and to follow this interaction in time. Because no effort was made to take into account the scalar interaction between the two types of spins, this approach was limited to proton DNP.

Here, the computational methodology for quantifying the contribution of the dipolar interaction to the ODNP effect is further developed to take into account the scalar interaction between the electron and nuclear spins. This is achieved by performing quantum mechanical (*ab initio*) calculations on the snapshots generated during the MD simulation. Unlike the dipolar interaction, which is long-ranged, the scalar interaction

[a] *Faculty of Engineering and Natural Sciences, Sabanc University, Orhanl-Tuzla, 34956 Istanbul, Turkey. E-mail: dsezer@sabanciuniv.edu*

[b] *Institute of Physics, Kazan Federal University, 420008 Kazan, Russian Federation*

† Electronic supplementary information (ESI) available. See DOI: 10.1039/c5cp04405g

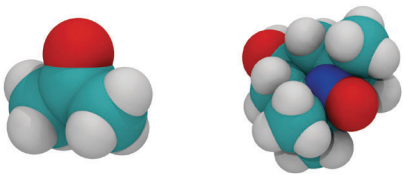

Fig. 1 Left: A molecule of acetone contains six hydrogen atoms (white), two methyl carbon atoms (cyan), one carbonyl carbon (cyan), and one oxygen atom (red). Right: The nitroxide free radical TEMPOL.

is influenced only by the molecular and liquid structure in the immediate neighborhood of the unpaired electron. Therefore, each *ab initio* calculation at a given time point only needs to contain a few molecules from the MD snapshot. In essence, we follow the dynamics of thousands of molecules in the liquid by classical MD simulations, and calculate the electron spin density at the nuclei of interest by performing *ab initio* calculations on a few molecules. This division of labor makes the approach efficient and realistically applicable to simple liquids.

In this paper, the proposed computational methodology is illustrated in the context of TEMPOL in pure acetone, for which we recently performed ^{1}H DNP analysis based on MD simulations.[25] In addition to protons, acetone offers two types of carbon nuclei: methyl carbon and carbonyl carbon (Fig. 1, left). We find differences in the contributions of scalar and dipolar interactions to the ODNP of these two types of ^{13}C nuclei. Furthermore, the protons of acetone allow us to examine the influence of proton polarization on the polarization of the carbon nuclear spins and, thus, quantify the magnitude of the three-spin effect.[2] For TEMPOL in pure acetone the effect of the proton spin on ^{13}C polarization is found to be negligibly small for most practical purposes.

The paper is organized as follows. In the next section we give general information about ODNP and the three-spin effect, and describe our methods. The dipolar contribution to ODNP is calculated in Section III.A. The calculation of the scalar interaction is presented in Section III.B. Combining these two contributions, we calculate DNP coupling factors in Section III.C and evaluate to what extent these would be modified by three-spin effects in Section III.D. The implications of the results are discussed in Section IV, while Section V contains our conclusion and outlook. Fitting parameters and other technical details are given in the ESI.†

II. Background and methods

A. Dipolar and scalar interactions

The Overhauser effect relies on the presence of hyperfine interaction between nuclear (I) and electron (S) spins. This interaction is described by the spin Hamiltonian[26] $H = \mathbf{I}\cdot\mathbf{A}\cdot\mathbf{S}$, where $\mathbf{I}$ and $\mathbf{S}$ are the respective spin operators and $\mathbf{A}$ is the hyperfine coupling tensor. The latter is composed of an isotropic (scalar) part A_{iso} and an anisotropic (dipolar) part $\mathbf{A}_{\mathrm{dip}}$. The anisotropic term, which is due to the dipolar interaction of the two spins, is a traceless tensor.[26] The isotropic term is known as Fermi contact or hyperfine coupling constant.[2,27] It is proportional to the electron spin density (*i.e.*, the difference of up-spin density and down-spin density) at the nucleus of interest and its value can be either negative or positive.[28]

In the presence of hyperfine coupling between I and S the relaxation of the longitudinal component of the nuclear spin magnetization is described by[2,26]

$$\frac{\mathrm{d}I}{\mathrm{d}t} = -\left(\rho_I^S + \omega_I\right)\left(I - I^0\right) - \sigma_I^S\left(S - S^0\right). \tag{1}$$

Here, upon overloading the notation, I and S denote the longitudinal components of the nuclear and electronic spin magnetizations. Their values at thermal equilibrium are indicated by a superscript zero. The self- and cross-relaxation rates, ρ_I^S and σ_I^S, are due to the hyperfine interaction between the spins, while ω_I is the nuclear T_1 rate in the absence of the electronic spin. At steady state the enhancement of the NMR signal, $e_I = (I - I^0)/I^0$, is directly proportional to the saturation of the electronic spin, $s = (S^0 - S)/S^0$. From (1) one finds that

$$e_I = \frac{\sigma_I^S}{\rho_I^S}\frac{\rho_I^S}{\rho_I^S + \omega_I}s\frac{\gamma_S}{\gamma_I} = c_I^S f_I^S s\frac{\gamma_S}{\gamma_I}. \tag{2}$$

The second equality in (2) defines the coupling factor

$$c_I^S = \sigma_I^S/\rho_I^S \tag{3}$$

and the leakage factor

$$f_I^S = \frac{\rho_I^S}{\rho_I^S + \omega_I}. \tag{4}$$

The relaxation rates σ_I^S and ρ_I^S in (3) can be calculated from the spectral density functions (SDFs) of the dipolar and scalar interactions between the spins:[2,21,26]

$$\sigma_I^S = N_S[5J_{IS}(\omega_S) - 6K_{IS}(\omega_S)]/12, \tag{5}$$

$$\rho_I^S = N_S[3J_{IS}(\omega_I) + 7J_{IS}(\omega_S) + 6K_{IS}(\omega_S)]/12. \tag{6}$$

Here, $J(\omega)$ and $K(\omega)$ denote the dipolar and scalar SDFs, respectively, ω_S and ω_I are the Larmor frequencies of the spins, and N_S is the number density of S. Note that in (5) and (6) we have acknowledged that $J(-\omega) = J(\omega)$, $K(-\omega) = K(\omega)$ and $\omega_S \gg \omega_I$.

Our computational strategy consists of following the molecular motions in time with MD simulations. The MD trajectories provide the positions of the spin-bearing atoms. Treating the spins as point dipoles, the atomic positions are used to calculate the dipolar time correlation function (TCF):

$$C_{\mathrm{dip}}(t) = \langle F_2^m(\tau)F_2^m(\tau + t)\rangle_\tau, \tag{7}$$

where $F_2^m = Y_2^m(\theta, \phi)/r^3$ is the rank-2 solid harmonic, and $\mathbf{r} = (r, \theta, \phi)$ is the vector from the electron to the nuclear spin in spherical coordinates. The brackets $\langle\cdot\rangle_\tau$ denote average over all starting times τ and over all nuclear spins in the simulation box. The dimension of the product of two solid harmonics is inverse volume squared (nm^{-6}). However, the average in (7) involves integration over volume, thus the dimension of the resultant C_{dip} is inverse volume (nm^{-3}). From the TCF we calculate the dipolar SDF as

$$J_{IS}(\omega) = \frac{2\pi}{5}(\delta_{IS})^2\int_0^\infty C_{\mathrm{dip}}(t)\mathrm{e}^{-\mathrm{i}\omega t}\mathrm{d}t, \tag{8}$$

where $\delta_{IS} = (\mu_0/4\pi)\hbar\gamma_I\gamma_S$ has a dimension of volume over time ($nm^3\ ns^{-1}$). Thus, the dimension of J_{IS} is volume over time ($nm^3\ ns^{-1}$), as it should be since it gives a relaxation rate (ns^{-1}) when multiplied by the number density N_S (nm^{-3}). For further details and applications of our computational approach the reader is referred to ref. 23–25.

Unlike the dipolar interaction, which could be treated in the point-dipole approximation, the calculation of the scalar interaction A_{iso} requires knowledge of the spin density of the unpaired electron of TEMPOL. Such information is not available in the classical MD simulations but necessitates quantum mechanical calculations. To this end, we used the atomic coordinates from the MD snapshots as an input to the package Gaussian[29] and calculated the Fermi contacts between the desired nuclei and the electron spin, A_{iso} (in MHz). These were used to obtain the scalar TCF

$$C_{iso}(t) = \frac{(2\pi)^2}{N_I}\langle A_{iso}(\tau)A_{iso}(\tau+t)\rangle_\tau, \tag{9}$$

where the prefactor is necessary to switch to units of angular frequency. Accumulated calculations are first time averaged and then divided by the number density of the spin I (Table 1). Since A_{iso} from the quantum mechanical package already includes the contribution of the gyromagnetic ratios, the scalar SDF is simply

$$K(\omega) = \int_0^\infty C_{iso}(t)e^{-i\omega t}dt. \tag{10}$$

Its dimension is volume over time ($nm^3\ ns^{-1}$). Additional information is available in the ESI† Section I.B.

B. Three-spin effect

The formalism summarized above applies to both ^1H and ^{13}C nuclei. However, when quantifying the ODNP enhancement of ^{13}C it may be necessary to take into consideration the additional interaction between carbon and proton nuclear spins. Thus, we allow for the polarization of the ^{13}C (third) spin to be influenced by the polarizations of the electron (first) and proton (second) spins, with the understanding that the polarization of the second spin is due to the first spin only. In this case, the relaxation of the longitudinal spin polarization of ^{13}C can be expressed as[2]

$$\begin{aligned}\frac{dI_C}{dt} = &-\left(\rho_C^S + \rho_C^H + \omega_C\right)\left(I_C - I_C^0\right) - \sigma_C^S\left(S - S^0\right)\\ &- \sigma_C^H\left(I_H - I_H^0\right),\end{aligned} \tag{11}$$

where the additional cross- and self-relaxation rates, σ_C^H and ρ_C^H, are due to carbon–proton coupling.

Table 1 Nuclear spin number densities, N_I, and concentrations, [I], for the MD simulations of acetone at 35 °C. [I] = N_I/N_A, where N_A is Avogadro's number

	C_{H_3}	C_O	H
N_I/nm^{-3}	16.13	8.06	48.39
[I]/M	26.8	13.4	80.4

At steady state, and assuming that carbon polarization does not affect proton polarization,[2] the enhancement of the ^{13}C signal, $e_C = (I_C - I_C^0)/I_C^0$, can be written as

$$e_C = \frac{\sigma_C^S - \sigma_C^H c_H^S f_H^S}{\rho_C^S + \rho_C^H + \omega_C} s\frac{\gamma_S}{\gamma_C}, \tag{12}$$

where c_H^S is the proton coupling factor as defined in (3) and f_H^S is the proton leakage factor as defined in (4). In terms of the carbon coupling factor, $c_C^S = \sigma_C^S/\rho_C^S$, and the leakage factor, $f_C^S = \rho_C^S/(\rho_C^S + \rho_C^H + \omega_C)$, the expression in (12) becomes

$$e_C = \left(mc_C^S\right)f_C^S s\frac{\gamma_S}{\gamma_C}, \tag{13}$$

where

$$m = 1 - \frac{\sigma_C^H}{\sigma_C^S}\left(c_H^S f_H^S\right) \tag{14}$$

is a multiplicative correction to the carbon coupling factor that accounts for the additional interaction of ^{13}C with the proton spins of the solvent.

An obvious prerequisite for having m significantly different from 1 is substantial enhancement of the proton signal, reflected by $(c_H^S f_H^S)$ in (14). Because the dipolar interaction typically dominates in proton DNP,[30] this product is expected to be positive. The second, more demanding requirement for appreciable three-spin effect is that the cross-relaxation rates σ_C^H and σ_C^S are comparable in magnitude, so that $\sigma_C^H/\sigma_C^S \sim 1$. The challenge lies in the fact that, from (5) and (8), σ_I^S is proportional to $(\gamma_I\gamma_S)^2$. Thus, considering the gyromagnetic ratios only, $\sigma_C^H/\sigma_C^S \sim (1/658)^2$, which is five orders of magnitude smaller than 1. However, from (5), σ_I^S is also proportional to the spin density N_S. Therefore, the second condition could be fulfilled if N_H is about five orders of magnitude larger than N_S. The proton density of pure acetone is [H] = 80 M (Table 1). Considering only the gyromagnetic ratios and the spin concentrations, for [S] = 1 mM we get $\sigma_C^H/\sigma_C^S \sim 0.2$.

In principle, the interaction between the ^{13}C and ^1H nuclear spins can have both dipolar and scalar (J-coupling) contributions. However, because the latter is limited to proton nuclei on the same molecule as the carbon nucleus of interest, it will not benefit from the concentration advantage ([H] ≫ [S]) that is necessary for the appreciable three-spin effect. Therefore, when calculating σ_C^H we considered only the dipolar coupling of ^{13}C to proton nuclei. Denoting the SDF of this dipolar interaction by J_{CH}, the cross-relaxation rate is[2,26]

$$\sigma_C^H = N_H[6J_{CH}(\omega_C + \omega_H) - J_{CH}(\omega_C - \omega_H)]/12. \tag{15}$$

Here we have both ω_H and ω_C because the Larmor frequencies of the two nuclei are not very different [*cf.* (5)].

One last factor that may contribute to larger three-spin effect is the frequency dependence of the cross-relaxation rates. In the ratio σ_C^H/σ_C^S the numerator relies on the SDF J_{CH} evaluated around the proton Larmor frequency ($\omega_H \pm \omega_C$), while the denominator relies on the SDF J_{CS} evaluated at the electron Larmor frequency (ω_S). The SDF at the higher frequency is expected to be much smaller in magnitude.

C. MD simulations and *ab initio* calculations

The MD simulations of the 1 TEMPOL molecule in a cubic box containing 2740 acetone molecules were reported previously.[25] The simulation parameters of acetone were obtained from ref. 31, and of TEMPOL were obtained from ref. 32. Constant-volume simulations were performed using NAMD[33] at 35 °C under periodic boundary conditions for a total duration of 10 ns. The integration time step was 2 fs and the coordinates were recorded every 0.2 ps.

Ab initio calculations were carried out on the molecular geometries from the MD snapshots. The packages Gaussian 09[29] and ORCA[34] were used at the B3LYP level of theory using the EPR-II basis set, which is known to produce reasonably good hyperfine coupling values.[35] Two separate fragments of the MD trajectory (located at the second and fifth nanosecond) were subjected to the analysis. Each fragment contained 1 ns of dynamics comprising 5000 successive snapshots. Thus, in total, 10 000 *ab initio* calculations were performed.

The spatial distribution of the spin density due to the unpaired electron of TEMPOL is expected to be sensitive to the immediate surroundings of the free radical. For a realistic representation of the environment, the *ab initio* calculations should include as many acetone molecules near TEMPOL as possible. However, considering the steep increase of the computational cost in *ab initio* calculations with the number of atoms, a reasonable number of solvent molecules had to be chosen. To this end, for one MD snapshot, the coordinates of the TEMPOL molecule and an increasing number of acetone molecules were provided as input to the *ab initio* calculation. The Fermi contact of the methyl carbon closest to the TEMPOL oxygen is shown in Fig. 2 for different numbers of acetone molecules (from 1 to 7) present in the calculations (red squares). The value of A_{iso} is seen to increase monotonically. The increase appears to slow down once six acetone molecules closest to TEMPOL are explicitly included in the *ab initio* calculation.

We further examined whether the dielectric properties of the acetone solution influence the calculated value of A_{iso}. The same molecular geometries were analyzed using the polarization continuum model (PCM)[36] implemented in Gaussian[37] (Fig. 1, black squares). Systematically higher Fermi contact values were obtained in the calculations using the PCM. More importantly, by using the PCM the A_{iso} values calculated with three and more explicit acetone molecules were practically identical, showing convergence of the Fermi contact with the number of molecules in the *ab initio* calculation. In the light of these observations, TEMPOL and the six acetone molecules closest to its oxygen atom were retained in all the other MD snapshots and subjected to an *ab initio* calculation using the PCM with the dielectric constant of acetone (ε = 20.5).

For the geometries that yielded the largest A_{iso} values among the 10 000 calculations, we further evaluated the effect of the basis set on the calculated Fermi contacts. The numerical values produced using the packages Gaussian and ORCA with the basis sets EPR-II, EPR-III and TZVP are compared in Fig. 3. There, the colored symbols correspond to nuclei on the acetone molecule closest to TEMPOL (shown in the inset). The grey symbols represent the same kind of nuclei on the remaining five acetone molecules present simultaneously in the same *ab initio* calculation. Different basis sets are observed to yield identical numerical values for carbon atoms. In the case of ^{1}H, the Fermi contact calculated using TZVP is slightly smaller than

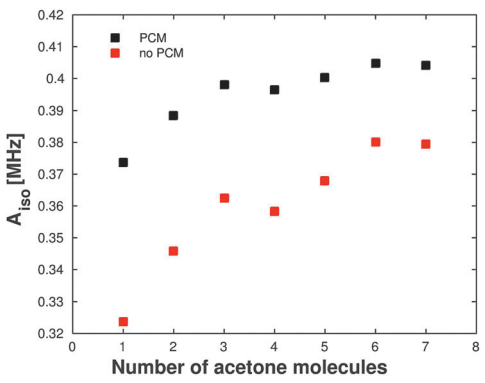

Fig. 2 Hyperfine coupling constants of a selected methyl carbon. The number of acetone molecules closest to the TEMPOL oxygen was increased from 1 to 7 in the *ab initio* calculations performed under vacuum (red squares) or using the polarization continuum model (black squares).

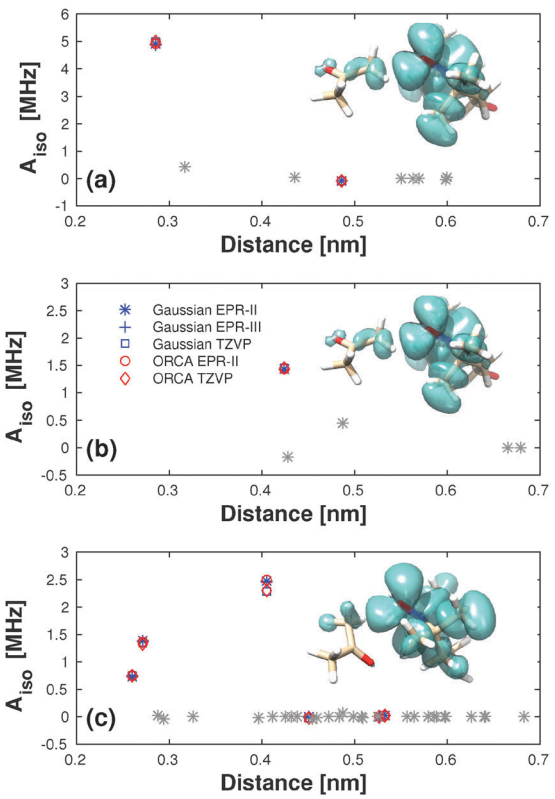

Fig. 3 Observed maximal Fermi contacts of (a) $^{13}C_{H_3}$, (b) $^{13}C_O$, and (c) ^{1}H. Different symbols show calculations using various basis sets. Colored and grey symbols represent the same kind of nuclei on, respectively, the closest (shown in inset) and more distant acetone molecules present in the same calculation. Insets show the positive electron spin densities for the corresponding configurations. C_{H_3} and C_O attain their maximum (positive) Fermi contacts in the same snapshot.

EPR-II for the maximum point but is identical for all the others. The insets in Fig. 3 show the positive part of the electron spin densities for these snapshots (generated using UCSF Chimera[38]).

III. Results

A. Dipolar interaction

Assuming that the DNP effect is entirely due to the dipolar coupling between the electron and nuclear spins, we recently reported ODNP coupling factors between the protons of acetone and TEMPOL, which were calculated from atomistic MD simulations.[25] Using the snapshots from these MD simulations, we conducted the same analysis—treating only the effect of dipolar coupling—for the carbon nuclear spins of the acetone solvent molecules. (See ESI,† Section I.A for the multi-scale calculation of the dipolar SDFs and Section II.A.1 for the values of the various parameters involved in the computational procedure.) The resulting DNP coupling factors for the methyl carbon (C_{H_3}) and the carbonyl carbon (C_O) of acetone are presented in Table 2,[39] which also contains the previously reported proton (H) coupling factors[25] for the purposes of comparison.

The dipolar coupling factor is known to be influenced by the translational diffusion of the spins and their distance of the closest approach, as made clear by the analytically-tractable model of hard spherical molecules with centered spins.[40,41] Being on the same molecule, we expect the translational diffusion of the carbon atoms of acetone to be the same as that for the acetone protons. However, because both the methyl and carbonyl carbon atoms are closer to the center of the acetone molecule than the protons (Fig. 1, left), the coupling factors of the former are expected to be somewhat smaller. This trend is confirmed by the calculated values in Table 2.

B. Scalar interaction

The values of the Fermi contacts from the *ab initio* calculations are shown in Fig. 4, where they are plotted against the distance between the TEMPOL oxygen and the respective acetone atom. Both positive and negative values occur for the three types of nuclei. While the largest positive values are larger in magnitude than the smallest negative values for the carbon atoms, positive and negative Fermi contacts of a similar absolute value are observed for the protons. Notably, the Fermi contacts do not change monotonically with the distance of the nucleus from the position of the oxygen atom of TEMPOL.

Table 2 DNP coupling factors (%) for ^{1}H and ^{13}C calculated at different electron Larmour frequencies (GHz) using only the dipolar interaction of electronic and nuclear spins

	9.7	34	94	200	260	330	460
C_{H_3}	35.4	17.8	6.54	2.58	1.84	1.33	0.81
C_O	34.4	15.3	4.37	1.48	1.00	0.70	0.41
H	36.2	20.0	9.38	4.51	3.48	2.78	2.04

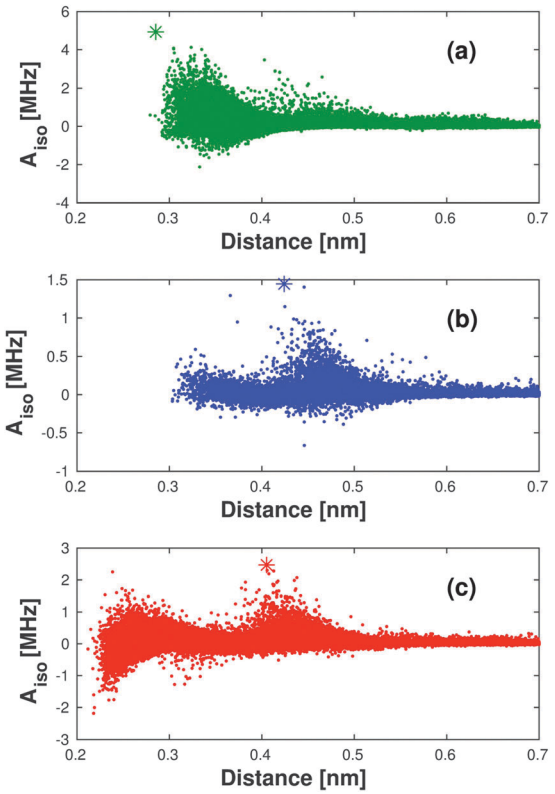

Fig. 4 Fermi contacts of (a) $^{13}C_{H_3}$, (b) $^{13}C_O$, and (c) ^{1}H nuclei of acetone against their distances to the TEMPOL oxygen. Maximum values are indicated with asterisk.

For the geometries leading to largest positive Fermi contacts (indicated by asterisk in Fig. 4) the positive part of the spin density is shown in the insets of Fig. 3. Methyl and carbonyl carbon atoms attain their maximum (positive) Fermi contacts in the same MD snapshot, as seen in Fig. 3a and b, whereas the maximum for protons is reached in a different MD snapshot (Fig. 3c). The molecular geometries and spin densities demonstrate how, for the acetone molecule closest to the unpaired electron of TEMPOL, the value of the spin density at the atomic nucleus does not scale with its distance from the TEMPOL oxygen. In Fig. 3c, for example, all the three protons of the methyl group closer to TEMPOL have positive Fermi contacts. However, the spin density at the proton farther from the TEMPOL oxygen is larger than the spin density at the closer proton, which is reflected in the magnitude of their Fermi contacts.

The scalar TCFs calculated from the A_{iso} values according to (9) are given in Fig. 5. A comparison across the three atom types reveals that C_{iso} of C_{H_3} (Fig. 5a) is an order of magnitude larger than C_O (Fig. 5b) and ^{1}H (Fig. 5c). The TCF of C_{H_3} also exhibits a slow decaying component of a relatively larger amplitude than the other two. In order to calculate SDFs from the TCFs the latter were fit to a multiexponential decay (as described in ESI,† Section I.B). The best fits, shown with dashed lines in Fig. 5, are found to be in very good agreement with the raw data. (Fitting parameters are given in the ESI,† Table S5.)

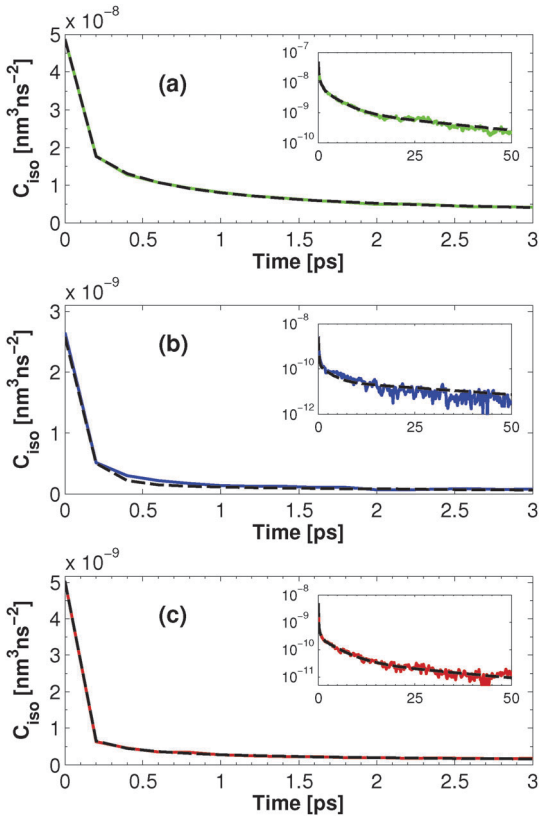

Fig. 5 Scalar TCFs calculated from the average of two trajectory fragments (solid) and multiexponential fits (dashed) for (a) C_{H_3}, (b) C_O and (c) H. Longer-time behavior is shown in insets.

Fig. 6 shows the scalar SDFs calculated as the Fourier transform of the multiexponential fits to the TCFs. As anticipated, $K(\omega)$ for C_{H_3} is larger than that of the other two nuclei. Because the SDF is affected by both the magnitude and the decay rate of the TCF, the longer tail of the C_{iso} of C_{H_3} leads to a larger difference in the SDFs, especially at the lower frequencies.

C. Coupling factors from scalar and dipolar interactions

The DNP coupling factor reflects the competition of the dipolar and scalar interactions between the electron and nuclear spins.

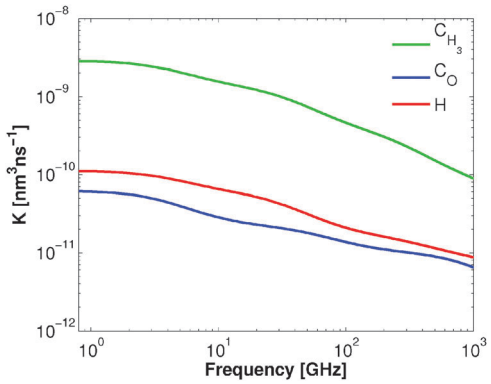

Fig. 6 Scalar SDFs for C_{H_3} (green), C_O (blue) and H (red).

At high magnetic fields $J(\omega_I) \gg J(\omega_S)$. If in addition $J(\omega_I) \gg K(\omega_S)$, the coupling factor becomes

$$c_I^S \approx \frac{5J_{IS}(\omega_S) - 6K_{IS}(\omega_S)}{3J_{IS}(\omega_I)}, \qquad (16)$$

where the approximation follows from (3), (5) and (6). Note that while the scalar SDF contributes only at the Larmor frequency of the electron, the dipolar SDF is probed at both the electron and nuclear Larmor frequencies. However, being in the denominator of (16), a larger $J(\omega_I)$ always decreases the magnitude of the coupling factor, independently of the competition between $J(\omega_S)$ and $K(\omega_S)$ in the numerator.

The dipolar and scalar SDFs, $J(\omega)$ and $K(\omega)$, are compared in Fig. 7 for the three atom types of interest. At the electronic Larmor frequencies (indicated with circles) the different nuclei exemplify different possibilities. In the case of ^{1}H (Fig. 7c), $J(\omega_S)$ completely dominates $K(\omega_S)$ over the entire frequency range, thus the DNP coupling factor is expected to be insensitive to the proton–electron Fermi contact. The situation is similar for $^{13}C_O$ (Fig. 7b); however, the difference between the dipolar and scalar SDFs is smaller. In contrast, for $^{13}C_{H_3}$ (Fig. 7a), $K(\omega_S)$ is almost equal to $J(\omega_S)$ at $\sim$94 GHz and exceeds it at higher frequencies. Because in (16) $K(\omega_S)$ is multiplied by 6 while $J(\omega_S)$ is multiplied by 5, we expect the two to balance exactly, and thus lead to vanishing of the DNP coupling factor, at frequencies of

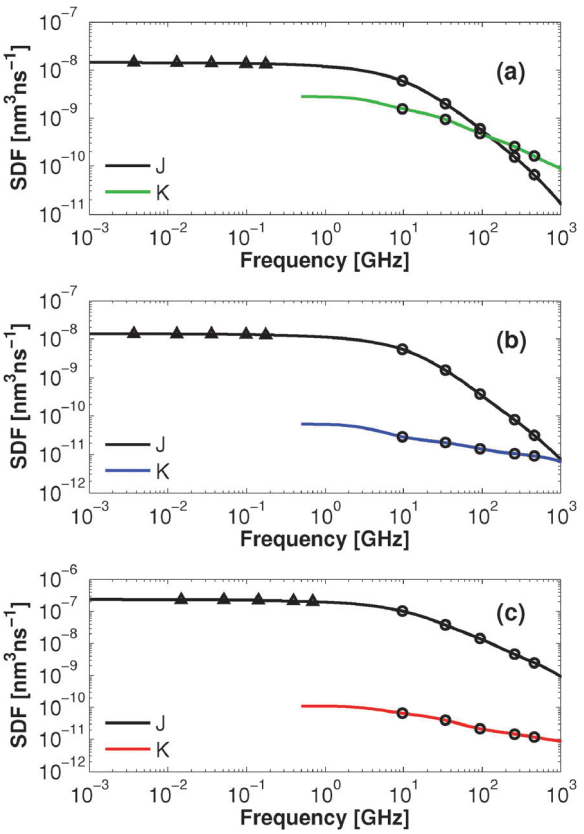

Fig. 7 Dipolar and scalar SDFs for (a) C_{H_3}, (b) C_O and (c) H. Symbols indicate the five electron (°) and nuclear (∇) Larmor frequencies reported in Table 3.

Table 3 DNP coupling factors (%) for various electron/proton Larmour frequencies (GHz/MHz) calculated by accounting for both dipolar and scalar interactions

	9.7/15	34/50	94/140	260/400	460/700
C_{H_3}	21.7	7.0	0.2	−1.7	−1.5
C_O	34.1	15.1	4.2	0.8	0.3
H	36.2	19.9	9.36	3.47	2.02

interest to medical MRI (50–70 GHz). At higher frequencies, as scalar SDF goes over the dipolar SDF, the sign of the coupling factor is expected to be changed.

Quantitative calculation of the DNP coupling factors according to (3), (5) and (6) confirms these expectations (Table 3). Comparison with the purely dipolar coupling factors in Table 2 makes clear that the scalar contribution to ^{1}H ODNP is negligible over the entire frequency range of experimental interest. In the case of $^{13}C_O$ scalar coupling can be safely ignored at the lower frequencies of interest; however, its effect starts being detrimental at higher frequencies. The opposite is true for $^{13}C_{H_3}$. Scalar coupling is detrimental at the lower frequencies, entirely canceling the dipolar contribution at ∼94 GHz. It becomes sufficiently large to produce comparable (but opposite in sign) enhancement at 260 GHz. At 460 GHz the coupling factor in the presence of both scalar and dipolar interactions is two times larger in magnitude than what would be possible with dipolar interaction only.

D. Three-spin effect

When both the ^{13}C and ^{1}H nuclei experience ODNP, the polarization of the latter has the potential to influence the polarization of the former. The extent to which the ^{13}C coupling coefficient will change due to this additional three-spin effect is determined by the multiplicative correction factor m defined in (14).

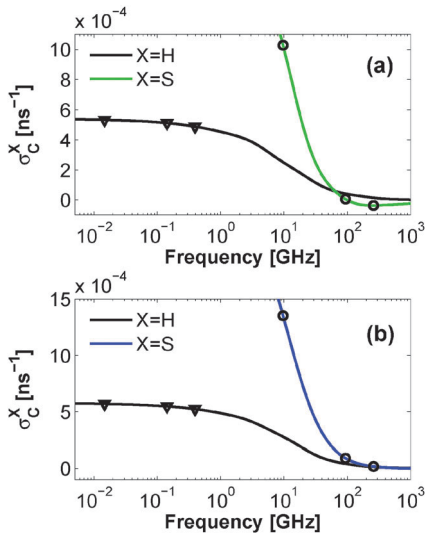

Fig. 8 Cross-relaxation rates of (a) C_{H_3} and (b) C_O. σ_C^H (black) is calculated for [H] = 80 M and σ_C^S (green/blue) is calculated for [S] = 1 mM. Symbols indicate the electron (°) and proton (∇) Larmor frequencies 9.7 GHz/15 MHz, 94 GHz/140 MHz and 260 GHz/400 MHz.

Fig. 8 shows the frequency dependence of the cross-relaxation rates σ_C^H (black) and σ_C^S (colored) calculated for, respectively, [H] = 80 M and [S] = 1 mM. At frequencies where the dipolar and scalar SDFs (shown in Fig. 7) become comparable in magnitude, σ_C^S is vanishingly small. The values of σ_C^S at 9.7 GHz, 94 GHz and 260 GHz are indicated with circles in Fig. 8. This cross-relaxation rate decreases sharply when going from 9.7 GHz to 94 GHz for both C_{H_3} (Fig. 8a) and C_O (Fig. 8b). In the case of the former, σ_C^S is negative at 260 GHz. Thus, from (14), the correction factor m is expected to be larger than 1 at 260 GHz.

The carbon–proton dipolar SDF was calculated in exactly the same way as the carbon–electron (and proton–electron[25]) SDFs. (The calculated SDFs and various fitting parameters are given in the ESI,† Section II.A.2.) The cross-relaxation rates σ_C^H obtained by appropriately normalizing the dipolar SDFs and multiplying by the proton density [H] = 80 M are shown in Fig. 8 with black lines. The magnitude of σ_C^H is found to be very similar for the magnetic fields of 0.34 T, 3.3 T and 9.2 T (indicated by ∇ in the figure).

The multiplicative three-spin correction factors at these three magnetic fields are plotted in Fig. 9 for C_{H_3} (left) and C_O (right). When calculating the ratio σ_C^H/σ_C^S the proton concentration was kept at [H] = 80 M while the TEMPOL concentration was varied from 1 mM to 20 mM. In addition, we used the ^{1}H coupling factor c_H^S from Table 3. Thus, we are in a position to calculate all factors in (14) except f_H^S. In Fig. 9, m is calculated for three different values of the proton leakage factor: f_H^S = 1 (black), f_H^S = 0.7 (dashed), and f_H^S = 0.4 (colored). Because f_H^S is proportional to the concentration of the polarizing agent, we can (arbitrarily) imagine these values to correspond to TEMPOL

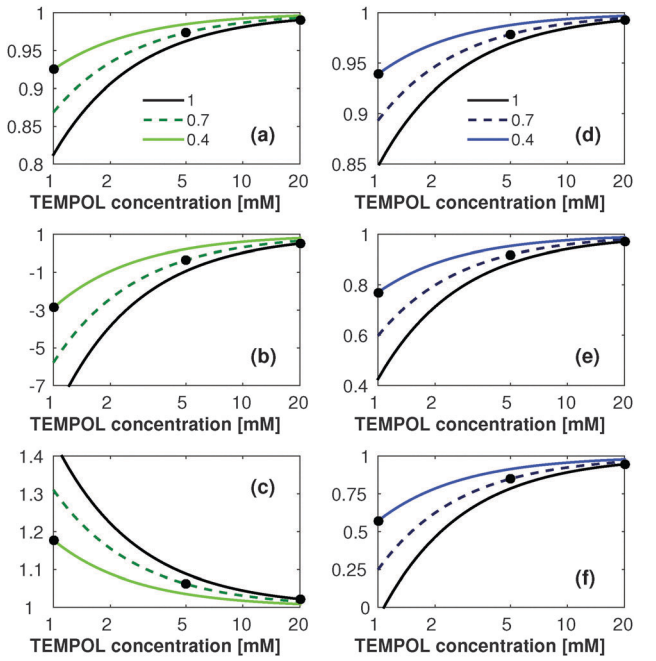

Fig. 9 Three-spin multiplicative correction factors, m, of C_{H_3} (left) and C_O (right) calculated at 9.7 GHz (a and d), 94 GHz (b and e), and 260 GHz (c and f). The examined proton leakage factors are f_H^S = 1 (black), 0.7 (dashed) and 0.4 (colored). Plausible leakage factors for the specified TEMPOL concentrations are indicated with black points.

concentrations of, respectively, 20 mM, 5 mM and 1 mM (indicated by black points in Fig. 9).

In all cases, at a TEMPOL concentration of 20 mM the ^{13}C coupling factor is essentially unaffected by the three-spin effect ($m \approx 1$). The influence is strongest at the lowest concentration of 1 mM, on which we focus now. For C_O (Fig. 9, right), the three-spin effect is predicted to reduce the coupling factor at all magnetic fields examined in the figure. The decrease can be as small as $\sim$5% at 9.7 GHz (Fig. 9d) and as large as $\sim$50% at 260 GHz (Fig. 9f). In the case of C_{H_3} (Fig. 9, left), the three-spin effect leads to a smaller (by $\sim$5%) coupling factor at 9.7 GHz (Fig. 9a) and to a larger coupling factor (by $\sim$20%) at 260 GHz (Fig. 9c). At 94 GHz (Fig. 9b), the three-spin effect flips the sign of the coupling factor and increases its magnitude by a factor of $\sim$300%. This huge three-spin effect is caused by the vanishingly small value of σ_C^S, by which σ_C^H is to be divided. However, because c_C^S is itself proportional to σ_C^S, the direct coupling factor of C_{H_3} is already rather small at 94 GHz (Table 3). Thus, its significant increase caused by the three-spin effect is not expected to be very helpful in practice.

IV. Discussion

The computational approach that was followed consisted of (i) performing MD simulations of the acetone liquid containing the polarizing agent TEMPOL, thus following the dynamics of $\sim$2700 molecules, and (ii) subjecting a small fraction of the molecules in the MD snapshots to quantum mechanical calculations. Relying on the point-dipole approximation, the atomic positions in the MD snapshots were used to calculate the dipolar SDF.[21,22] At this stage, finite-size corrections to the SDF were introduced as previously described.[23,24] The novelty of the present paper is the subsequent use of the MD snapshots in the *ab initio* calculation of the Fermi contact interactions. By using the polarization continuum model, converged scalar couplings were obtained with only a few molecules included explicitly in the *ab initio* calculations (Fig. 2). The small number of molecules present in each quantum mechanical calculation (6 acetone and 1 TEMPOL) allowed us to calculate Fermi contacts from 10 000 different MD snapshots, thus ensuring the statistical convergence of the results.

Considering only the contribution of the electron–nuclear dipolar interaction, the ^{13}C DNP coupling factors at the lower fields (<3 T) were not much smaller than those of protons (Table 2). Because the translational diffusion of the carbon and proton nuclei is dictated by the acetone molecule to which they belong, this result is not surprising. The effect of the ''distance of closest approach'' on the dipolar coupling factors of the three nuclei was also observed in Table 2. While protons had largest dipolar coupling factors, the most centrally located atom C_O had smallest dipolar coupling factors, and those of C_{H_3} were in between. Differences in the proximity of the atoms to the surface of the molecule were observed to have increasingly larger effect on the dipolar coupling factors at higher magnetic fields (>3 T).

The Fermi contacts calculated for the three types of nuclei exhibited both positive and negative values during the dynamics of the molecules (Fig. 4). As a result, a fast (sub ps) decay of the scalar TCFs was observed for all the three studied nuclei (Fig. 5). In addition, at distances less than about 4 Å, the magnitude of A_{iso} did not change monotonically with the separation of the nucleus from the TEMPOL oxygen (Fig. 4). These findings should be contrasted with the expressions of a Fermi contact interaction decaying exponentially with distance that have been used in the literature.[19,42,43] Clearly, due to the complex dependence of the spin density on the intermolecular geometry (Fig. 3, insets), the reliable prediction of the scalar interaction appears to require the use of quantum mechanical calculations, as was done in the present work.

Distinct scalar SDFs were obtained for the three nuclei (Fig. 6). Interestingly, although the acetone protons almost always come closer to the unpaired electron compared to the central acetone carbon (C_O), the scalar SDF of the former nuclear spin was not much larger than that of the latter. In comparison, the scalar SDF of the acetone methyl carbon (C_{H_3}) was determined to be more than an order of magnitude larger than the others across the entire frequency range shown in Fig. 6. Whatever its magnitude, however, to influence the Overhauser DNP the scalar SDF should be comparable to the dipolar SDF.

For the protons of acetone the dipolar SDF was found to be several orders of magnitude larger than the scalar SDF at all studied frequencies (Fig. 7). As a result, the scalar interaction had a negligible influence on the DNP coupling factors (Tables 2 and 3). Because the dipolar SDF scales with the square of the gyromagnetic ratio, the $J(\omega)$ values of the two types of carbon atoms of acetone were more than an order of magnitude smaller than that of the protons (Fig. 6). This allowed the scalar SDF of the carbonyl carbon, which was smaller than the proton $K(\omega)$, to come close to its dipolar SDF at high frequencies. The result was a significant cancellation of the respective enhancements and miserable C_O DNP coupling factors at frequencies higher than about 200 GHz (Table 3). At fields lower than about 4 T, however, the scalar interaction did not do much harm to the coupling factors, suggesting that appreciable enhancements of the carbonyl carbon NMR signal should be achievable through ODNP.

For the methyl carbon, which had the largest $K(\omega)$ among the three nuclei (Fig. 6), the scalar and dipolar SDFs were comparable in magnitude. Upon the increase of frequency the two SDFs were found to decrease with different rates and intersect at about 100 GHz (Fig. 7), at which point the coupling factor dropped to zero (Table 3). Due to the difference in their slopes, the scalar SDF dominates at higher frequencies leading to negative coupling factors (*i.e.*, positive enhancements). The slower decrease of $K(\omega)$ with frequency compared to $J(\omega)$ results in very similar scalar-dominated coupling factors at 260 GHz and 460 GHz for C_{H_3} (Table 3). This finding illustrates that at sufficiently high fields, where the scalar interaction dominates over the dipolar interaction at the electron Larmor frequency, the DNP coupling factor almost stops dropping with the field.[44]

We further investigated the influence of proton polarization on carbon polarization within the approximations of the three-spin treatment in ref. 2. To this end, the SDF of the proton–carbon dipolar interaction was calculated from the MD trajectories following the same procedure that was used to calculate the electron–carbon dipolar SDF. This allowed us to calculate the cross-relaxation rate σ_C^H as a function of frequency (Fig. 8). The calculation of σ_C^H illustrates that the multiscale treatment of the dipolar interaction, although developed keeping the Overhauser effect in mind, is directly applicable to the nuclear Overhauser effect, thus should be of interest for the calculation of intermolecular NOE in liquids.[45] Our detailed calculations demonstrated that the net NMR enhancement may either suffer or benefit from the three-spin effect depending on the type of ^{13}C nucleus and the DNP frequency (Fig. 9). However, for the carbon atoms of acetone the three-spin effect is not expected to play a significant role in practice. For completeness, it should be mentioned that the potential contribution of the proton–carbon *J*-coupling to the three-spin effect was deemed negligible and was ignored in our treatment.

Previously, we reported DNP coupling factors for acetone protons and TEMPOL, which were calculated disregarding the possibility of scalar interaction.[25] Our computational prediction of c = 3.5% at 260 GHz was larger than the experimental value of $\sim$2%.[15] However, the TEMPOL concentration in the experiment was 1 M, while the MD simulations were performed with one TEMPOL molecule in a box of acetone. MD simulations with 1 M TEMPOL resulted in a coupling factor of 2.9%, which is larger than the experimental value by a factor of $\sim$1.5. At the time we speculated that the inconsistency might be due to neglecting the scalar interaction in the computational analysis. Here, we demonstrated that for low TEMPOL concentration the proton coupling factors are not affected by the scalar interaction. We expect this conclusion to apply to high radical concentrations as well. Thus, the discrepancy between calculations and experiment reported in ref. 25 remains unexplained.

An experimental study by Lingwood *et al.* has reported room-temperature ^{13}C ODNP at 0.35 T.[18] The free radical 4-amino-TEMPO was introduced in a solution of water containing 5 M acetone. NMR signal enhancements (scaled by an arbitrary constant and corrected for three-spin effect and leakage factor) of -91 and -23 were reported for C_O and C_{H_3}, respectively.[18] In qualitative agreement, we found that at 9.7 GHz the coupling factor of C_O is larger than that of C_{H_3} (Table 3). However, while the enhancements of the two carbon types differ by a factor of $\sim$4 in the experiment, the ratio of the coupling factors we found is $\sim$1.6. In ref. 18, proton decoupling has been applied to investigate the contribution of the three-spin effect. Upon decoupling, *i.e.*, removing the three-spin effect, the NMR signal in the presence of 20 mM free radical has been reported to increase by $\sim$10% and $\sim$20% for C_O and C_{H_3}, respectively. In qualitative agreement, we also predict a slightly larger three-spin effect for C_{H_3} at 9.7 GHz (Fig. 9, top). However, we only reach a comparable magnitude of the three-spin effect at a much lower TEMPOL concentration (*e.g.*, 1 mM).

With all that said, quantitative agreement between our calculations and the findings of ref. 18 should not be expected because of several reasons. While we have modeled pure acetone at 35 °C, the experiment is performed by taking 5 M acetone in water (*i.e.*, $\sim$36 M water) at room temperature. The diffusion constants of the species should be affected by this difference in the physical conditions. Because the proton density of the water–acetone mixture is $\sim$100 M, whereas it is 80 M for pure acetone (Table 1), the three-spin effect in the experiment is expected to be larger than our calculations by at least a factor of 1.25. Finally, while similar to TEMPOL, the free radical 4-amino-TEMPO used in the experiment is expected to have an electric charge of +1e at pH 7. It is hard to speculate how this could influence the electron spin density at the position of the carbon atoms on acetone. The Fermi contacts should be further affected by the differences in the dielectric constants of the liquids: $\sim$60 for the water–acetone mixture *vs.* $\sim$20 for pure acetone.

One last remark is in order regarding the *ab initio* calculation of Fermi contacts from the molecular geometries in the MD snapshots. The B3LYP/ERP-II combination that we employed has been studied extensively in terms of its ability to produce high-quality Zeeman and hyperfine coupling tensors for nitroxide radicals.[46] The isotropic part of the latter, which is essentially the Fermi-contact interaction of the electron spin with the nitrogen of the nitroxide, has been found to be quite sensitive to the degree of pyramidality at the nitrogen and the exact length of the nitrogen–oxygen covalent bond.[47] Because in our case the molecular structures come directly from the classical MD simulations, the bond length and the bending of the nitrogen–oxygen bond relative to the nitroxide ring are expected to show variations—which are not necessarily realistic—across the MD snapshots. In principle, this may have adverse effect on the calculated Fermi contacts. However, the tests in the literature have focused on intramolecular Fermi contacts, whereas the Fermi contacts utilized in the presented approach are intermolecular and, thus, should be less sensitive to the precise geometry of the nitroxide.

V. Conclusion and outlook

A computational methodology for predicting Overhauser DNP coupling factors by accounting for the simultaneous presence of dipolar and scalar interactions between electron and nuclear spins was presented. It was applied to liquid acetone doped with TEMPOL. In addition to ^1H nuclei, whose DNP had been studied computationally before,[25] acetone contains two different types of carbon atoms: methyl carbon and carbonyl carbon. As both scalar and dipolar interactions are known to contribute to the ^{13}C DNP enhancement,[3] the developed approach made possible the prediction of the coupling factors of these two carbon nuclei over a wide range of magnetic fields.

Our results demonstrated that, for protons, the scalar interaction is not effective in liquid DNP and will remain ineffective for all high magnetic fields that may be reachable in the near future. Thus, proton ODNP is doomed to rely on the dipolar interaction for which the coupling factor is known to diminish

substantially with frequency. In contrast, for carbon atoms, the scalar interaction was found to be important at all fields beyond ~3 T. For the carbonyl carbon of acetone, the scalar interaction was shown to be unfavorable at fields higher than ~3 T. For the methyl carbon of acetone, the scalar interaction completely destroyed the NMR signal in the vicinity of ~4 T but was predicted to produce positive enhancements at fields beyond 9 T. Very encouragingly from the perspective of high-field liquid DNP, because of the slower decay of the scalar SDF with frequency (compared to the dipolar SDF), the positive enhancement is expected to remain almost unchanged when going from 400 MHz to 700 MHz (proton frequency).

On the basis of these results we can predict that, due to its reliance on the dipolar interaction, proton ODNP beyond 500 MHz may not be particularly rewarding as far as enhancing the NMR signal is concerned. In contrast, in the case of carbon atoms, liquid ODNP spectrometers at these higher fields have the potential to benefit tremendously from the scalar interaction because its spectral intensity drops more slowly with frequency compared to that of the dipolar interaction. However, the practical applications of ^{13}C ODNP at such high fields will require a better understanding of how the chemical type of carbon (*e.g.*, methyl carbon *vs.* carbonyl carbon) determines the strength of the scalar interaction. Among different carbon atoms, the dominance of scalar over dipolar interaction in liquid DNP at lower fields has been found to be largest for sp^3 hybridized carbon atoms bonded to chlorine atoms, as exemplified by chloroform.[3] We are in the process of applying the presented methodology to TEMPOL in chloroform. Our results will be reported in due course.

Acknowledgements

This work was supported by TUBITAK Research Grant No. 112T770 to D.S. S.E.K. is a recipient of a TUBITAK-BIDEP scholarship. The COST action TD1103 on Hyperpolarization Physics and Methodology in NMR and MRI is gratefully acknowledged.

References

1 C. Griesinger, M. Bennati, H. M. Vieth, C. Luchinat, G. Parigi, P. Höfer, F. Engelke, S. J. Glaser, V. Denysenkov and T. F. Prisner, *Prog. Nucl. Magn. Reson. Spectrosc.*, 2012, **64**, 4.
2 K. H. Hausser and D. Stehlik, *Adv. Magn. Reson.*, 1968, **3**, 79.
3 W. Müller-Warmuth and K. Meise-Gresch, *Adv. Magn. Reson.*, 1983, **11**, 1.
4 H. H. Fischer, M. Seiler, T. S. Ertl, U. Eberhardinger, H. Bertagnolli, H. Schmitt-Willich and K. Albert, *J. Phys. Chem. B*, 2003, **107**, 4879.
5 J. G. Krummenacker, V. P. Denysenkov, M. Terekhov, L. M. Schreiber and T. F. Prisner, *J. Magn. Reson.*, 2012, **215**, 94.
6 S. Ebert, A. Amar, C. Bauer, M. Kölzer, P. Blümler, H. Spiess, D. Hinderberger and K. Münnemann, *Appl. Magn. Reson.*, 2012, **43**, 195.
7 B. D. Armstrong, J. Choi, C. López, D. A. Wesener, W. Hubbell, S. Cavagnero and S. Han, *J. Am. Chem. Soc.*, 2011, **133**, 5987.
8 R. Kausik and S. Han, *Phys. Chem. Chem. Phys.*, 2011, **13**, 7732.
9 J. M. Franck, A. Pavlova, J. A. Scott and S. Han, *Prog. Nucl. Magn. Reson. Spectrosc.*, 2013, **74**, 33.
10 M. Reese, M.-T. Türke, I. Tkach, G. Parigi, C. Luchinat, T. Marquardsen, A. Tavernier, P. Höfer, F. Engelke, C. Griesinger and M. Bennati, *J. Am. Chem. Soc.*, 2009, **131**, 15086.
11 M. J. Prandolini, V. P. Denysenkov, M. Gafurov, B. Endeward and T. F. Prisner, *J. Am. Chem. Soc.*, 2009, **131**, 6090.
12 M.-T. Türke, I. Tkach, M. Reese, P. Höfer and M. Bennati, *Phys. Chem. Chem. Phys.*, 2010, **12**, 5893.
13 G. H. A. van der Heijden, A. P. M. Kentgens and P. J. M. van Bentum, *Phys. Chem. Chem. Phys.*, 2014, **16**, 8493.
14 P. Neugebauer, J. G. Krummenacker, V. P. Denysenkov, G. Parigi, C. Luchinat and T. F. Prisner, *Phys. Chem. Chem. Phys.*, 2013, **15**, 6049.
15 P. Neugebauer, J. G. Krummenacker, V. P. Denysenkov, C. Helmling, C. Luchinat, G. Parigi and T. F. Prisner, *Phys. Chem. Chem. Phys.*, 2014, **16**, 18781.
16 S. Stevenson, T. Glass and H. C. Dorn, *Anal. Chem.*, 1998, **70**, 2623.
17 P. Höfer, P. Carl, G. Guthausen, T. Prisner, M. Reese, T. Carlomagno, C. Griesinger and M. Bennati, *Appl. Magn. Reson.*, 2008, **34**, 393.
18 M. D. Lingwood and S. Han, *J. Magn. Reson.*, 2009, **201**, 137.
19 O. Neudert, C. Mattea, H. W. Spiess, S. Stapf and K. Münnemann, *Phys. Chem. Chem. Phys.*, 2013, **15**, 20717.
20 O. Neudert, C. Mattea, S. Stapf, M. Reh, H. W. Spiess and K. Münnemann, *Microporous Mesoporous Mater.*, 2015, **205**, 70.
21 D. Sezer, M. J. Prandolini and T. F. Prisner, *Phys. Chem. Chem. Phys.*, 2009, **11**, 6626.
22 D. Sezer, M. Gafurov, M. J. Prandolini, V. P. Denysenkov and T. F. Prisner, *Phys. Chem. Chem. Phys.*, 2009, **11**, 6638.
23 D. Sezer, *Phys. Chem. Chem. Phys.*, 2013, **15**, 526.
24 D. Sezer, *Phys. Chem. Chem. Phys.*, 2014, **16**, 1022.
25 S. E. Kücük, P. Neugebauer, T. F. Prisner and D. Sezer, *Phys. Chem. Chem. Phys.*, 2015, **17**, 6618.
26 A. Abragam, *The Principles of Nuclear Magnetism*, Oxford University Press, New York, 1961.
27 N. M. Atherton, *Principles of Electron Spin Resonance*, Ellis Horwood PTR Prentice Hall, 1993.
28 O. F. Schirmer, *J. Phys. C: Solid State Phys.*, 1973, **6**, 300.
29 M. J. Frisch, G. W. Trucks, H. B. Schlegel, G. E. Scuseria, M. A. Robb, J. R. Cheeseman, G. Scalmani, V. Barone, B. Mennucci, G. A. Petersson, H. Nakatsuji, M. Caricato, X. Li, H. P. Hratchian, A. F. Izmaylov, J. Bloino, G. Zheng, J. L. Sonnenberg, M. Hada, M. Ehara, K. Toyota, R. Fukuda, J. Hasegawa, M. Ishida, T. Nakajima, Y. Honda, O. Kitao, H. Nakai, T. Vreven, J. A. Montgomery, Jr., J. E. Peralta, F. Ogliaro, M. Bearpark, J. J. Heyd, E. Brothers, K. N. Kudin, V. N. Staroverov, R. Kobayashi, J. Normand, K. Raghavachari, A. Rendell, J. C. Burant, S. S. Iyengar,

J. Tomasi, M. Cossi, N. Rega, J. M. Millam, M. Klene, J. E. Knox, J. B. Cross, V. Bakken, C. Adamo, J. Jaramillo, R. Gomperts, R. E. Stratmann, O. Yazyev, A. J. Austin, R. Cammi, C. Pomelli, J. W. Ochterski, R. L. Martin, K. Morokuma, V. G. Zakrzewski, G. A. Voth, P. Salvador, J. J. Dannenberg, S. Dapprich, A. D. Daniels, Ö. Farkas, J. B. Foresman, J. V. Ortiz, J. Cioslowski and D. J. Fox, *Gaussian09 Revision D.01*, Gaussian Inc., Wallingford CT, 2009.

30 X. Wang, W. C. Isley III, S. I. Salido, Z. Sun, L. Song, K. H. Tsai, C. J. Cramer and H. C. Dorn, *Chem. Sci.*, 2015, DOI: 10.1039/C5SC02499D.

31 K. Vanommeslaeghe, E. Hatcher, C. Acharya, S. Kundu, S. Zhong, J. Shim, E. Darian, O. Guvench, P. Lopes, I. Vorobyov and A. D. Mackerell, *J. Comput. Chem.*, 2010, **31**, 671.

32 D. Sezer, J. H. Freed and B. Roux, *J. Phys. Chem. B*, 2008, **112**, 5755.

33 J. C. Phillips, R. Braun, W. Wang, J. Gumbart, E. Tajkorshid, E. Villa, C. Chipot, R. D. Skeel, L. Kale and K. Schulten, *J. Comput. Chem.*, 2005, **26**, 1781.

34 F. Neese, *Wiley Interdiscip. Rev.: Comput. Mol. Sci.*, 2012, **2**, 73.

35 V. Barone, in *Recent advances in density functional methods, part I*, ed. D. Chong, World Scientific Publ. Co., Singapore, 1997, ch. 8, pp. 287–334.

36 J. Tomasi, B. Mennucci and R. Cammi, *Chem. Rev.*, 2005, **105**, 2999.

37 V. Barone, M. Cossi and J. Tomasi, *J. Comput. Chem.*, 1998, **19**, 404.

38 E. F. Pettersen, T. D. Goddard, C. C. Huang, G. S. Couch, D. M. Greenblatt, E. C. Meng and T. E. Ferrin, *J. Comput. Chem.*, 2004, **25**, 1605.

39 The coupling factors in Table 2 are calculated from (3), entirely disregarding $K(\omega)$ in the expressions of σ_I^S, (5), and ρ_I^S, (6).

40 Y. Ayant, E. Belorizky, J. Alizon and J. Gallice, *J. Phys.*, 1975, **36**, 991.

41 L.-P. Hwang and J. H. Freed, *J. Chem. Phys.*, 1975, **63**, 4017.

42 J. B. Pedersen and J. H. Freed, *J. Chem. Phys.*, 1973, **58**, 2746.

43 P. Fries and E. Belorizky, *J. Phys.*, 1989, **50**, 3347.

44 This is not the same as ignoring $J(\omega)$ in the expression of the coupling factor and deducing $c \approx -1$ irrespective of the field. In our case, the denominator of c is still dominated by $J(\omega)$ at the nuclear Larmor frequency, as written in (16).

45 S. Gabl, C. Schröder, D. Braun, H. Weingärtner and O. Steinhauser, *J. Chem. Phys.*, 2014, **140**, 184503.

46 R. Improta and V. Barone, *Chem. Rev.*, 2004, **104**, 1231.

47 M. Pavone, P. Cimino, O. Crescenzi, A. Sillanpää and V. Barone, *J. Phys. Chem. B*, 2007, **111**, 8928.

